20th European Conference on Fracture (ECF20)

A lattice-spring model for damage evolution in cement paste

Mingzhong Zhang[a],*, Craig N Morrison[a,b], Andrey P Jivkov[a]

[a]*Mechanics and Physics of Solids Research Group, Modelling and Simulation Centre, The University of Manchester, Oxford Road, Manchester M13 9PL, UK*
[b]*Nuclear FiRST Doctoral Training Centre, The University of Manchester, Oxford Road, Manchester M13 9PL, UK*

Abstract

To understand better the fracture processes in cement-based materials, it is essential to predict the evolution of damage in cement paste. A recently proposed site-bond model is developed further to take into account the key microstructure data, such as pore size distribution, porosity, and size distribution and volume fraction of anhydrous cement grains obtained from high resolution X-ray tomography. The grains are associated with lattice sites linked by deformable bonds. The bonds are bundles of elastic-brittle springs, resisting normal and shear relative displacements between grains with potential for failure. The model length scale and thence spring constants are controlled by grain statistics. The spring failure properties are controlled by pore statistics. Macroscopic damage develops by a succession of local failures, represented by spring removal. The model is used to simulate the stress-strain response and damage in cement paste under uniaxial tensile loading. The influence of porosity on tensile strength and damage evolution is estimated in a quantitative manner. The predictions of the model are in a very good agreement with the available experimental data.

Keywords: Damage evolution; Cement paste; Site-bond model; Microstructure; Quasi-brittle behaviour

1. Introduction

Cement paste is a binder for cement-based materials and plays a critical role in their engineering-scale properties. Realistic predictions of fracture in such materials require understanding and modelling of damage evolution of

---

* Corresponding author. Tel.: +44(0)161 275 4306; fax: +44(0)161 275 4306.
  E-mail address: mingzhong.zhang@manchester.ac.uk

cement paste. This evolution results from progressive local failures and depends on the complex heterogeneous microstructure of the cement paste. Meso-scale mechanical models, accounting for heterogeneity, have been used to study the fracture process in cement-based materials (Schlangen and Qian, 2009). Discrete lattice models are amongst the promising approaches to represent generation and growth of local failures (Jivkov et al., 2013). Lately, a novel concept of site-bond assembly has been proposed by Jivkov and Yates (2012) and further developed to simulate the damage evolution in quasi-brittle materials accounting for microstructure by using lattice beam elements (Jivkov et al., 2013) and lattice spring elements (Jivkov et al., 2014; Zhang et al., 2014), respectively.

The main purpose of this work is to apply the proposed lattice-spring model to simulate the mechanical properties and damage evolution in hardened cement paste taking into account its microstructural characteristics, such as pore size distribution, porosity, and volume fraction and size distribution of anhydrous cement grains. These features are derived from high-resolution micro-computed tomography (micro-CT) scans based on a series of image processing and analysis. The 3D microstructure of cement paste comprised of anhydrous cement grains, hydration products and pores is represented by an assembly of truncated octahedral cells with sites at cell centres and bonds linking the neighboring cells. The simulated site-bond assembly is subjected to uniaxial tensile loading and damage evolution in cement paste is obtained. The simulation results are compared with the available experimental data.

2. 3D microstructure of hardened cement paste

The 3D microstructures of hardened cement paste used in this work were obtained from X-ray micro-CT scans, which were performed at University of Illinois at Urbana-Champaign (UIUC, USA). ASTM type I Portland cement was used. The w/c ratio of the cement paste specimen was 0.5 (mass ratio). After mixing, the paste was injected into a plastic tube (250 µm in diameter) using a syringe. The specimens were stored under standard curing conditions and scanned at 1, 7 and 28 days. More details on the X-ray micro-CT test can be found in (Zhang et al. 2012).

Fig. 1 shows the micro-CT image of a region of interest (ROI) with 200 µm in diameter and 100 µm in thickness extracted from the reconstructed 3D image of the 28-day old cement paste. The image resolution was 0.5 µm/voxel. Some features of different phases, i.e. anhydrous cement grains, hydration products and pores can be seen from this figure. Anhydrous cement grains with high density are shown in white. Pore space with low density is shown in black. The gray voxels most probably represent hydration products.
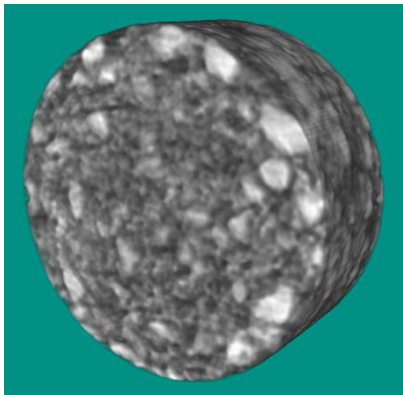

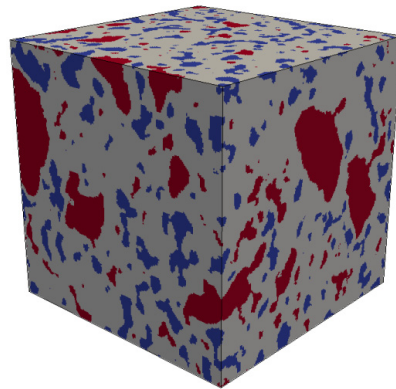Fig. 1. Micro-CT image of ROI of 28-day old cement paste.   Fig. 2. 3D microstructure of VOI of 28-day old cement paste.

The threshold gray values were determined based on the gray-level histogram to identify these three phases. Fig. 2 shows an example of the 3D microstructure of volume of interest (VOI) of cement paste as a result of image segmentation. It can be seen that the original image is converted into a ternary image of blue, light grey and dark red phases, which represent capillary pores, hydration products and anhydrous cement grains, respectively.

From image analysis, the microstructural characteristics, such as porosity, pore size distribution, and volume fraction and size distribution of anhydrous cement grains of ROI can be captured. For 28-day old cement paste,

porosity and volume fraction of anhydrous cement grains were found to be 12.58% and 8.65%, respectively. The obtained pore size distribution and size distribution of anhydrous cement grains are shown in Fig. 3.
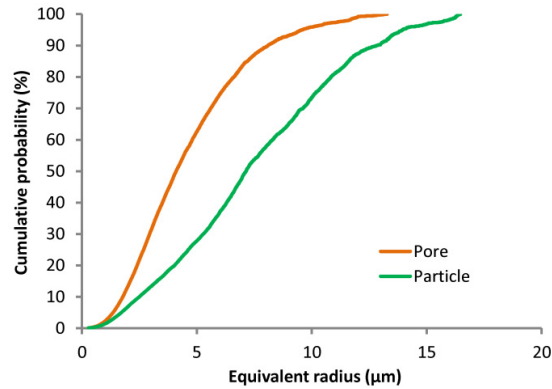

Fig. 3. Pore size distribution and particle size distribution of ROI of 28-day old cement paste.

3. Microstructure-informed modelling and simulation

In the site-bond model, the microstructure of a material is represented by an assembly of truncated octahedral cells, as shown in Fig. 4a. Each unit cell consists of six square and eight regular hexagonal faces. The cell centre is considered to be a site linking to its neighbouring sites by fourteen bonds, i.e., six bonds B_1 in principal directions through square faces and eight bonds B_2 in octahedral direction through hexagonal faces, as plotted in Fig. 4b. The bonds are modelled with elastic-brittle normal and shear springs to represent the relative deformations between adjacent cells, as illustrated in Fig. 4c. Based on the equivalence of the strain energy density of the discrete cell to the continuum system, the spring constants are derived as follows (Zhang et al., 2014):

$$k_n^p = \frac{EL}{4(1+v)(1-2v)}; \qquad k_s^p = 0; \qquad k_n^o = \frac{(1+2v)EL}{4(1+v)(1-2v)}; \qquad k_s^o = \frac{(1-4v)EL}{4(1+v)(1-2v)} \tag{1}$$

where k_n^p and k_s^p denote the stiffness coefficients of normal and shear springs in principal direction, k_n^o and k_s^o are the stiffness coefficients of normal and shear springs in octahedral direction, E and v are Young's modulus and Poisson's ratio of the material respectively, L is the spacing between two adjacent sites in principal directions.

The measured microstructural information is then incorporated into the site-bond model. Firstly, anhydrous cement grains of different sizes are randomly distributed to all sites of the cellular structure according to the particle size distribution as shown in Fig. 3. As a result, each cell has one spherical anhydrous cement grain with radius of R_i. The length scale, i.e. cell size (L), is calculated from the volume fraction of anhydrous cement grains (ϕ_a) and the volume of the cellular structure with N cells via $\phi_a NL^3/2 = \sum_i 4\pi R_i^3/3$. Secondly, on basis of the measured pore size distribution, pores are randomly assigned to the bonds (faces of cellular structure) until the known porosity is achieved. The critical failure energy of each bond is calculated by multiplying the surface energy (γ) by the effective surface area, i.e. the intact surface area minus pore area on the surface. Table 1 lists the input parameters for simulation in this work. A detailed description of the microstructure-informed site-bond model and failure criteria for springs is given in (Jivkov et al., 2014; Zhang and Jivkov, 2014). To quantify the evolution of damage of hardened cement paste under loading, a damage variable D_E is defined as the relative change in Young's modulus.
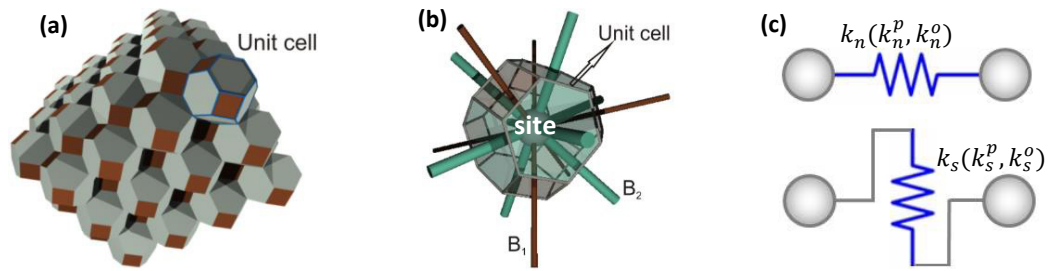
Fig. 4. Cellular lattice: (a) site-bond assembly; (b) unit cell with bonds; (c) normal and shear springs.

Table 1. Input parameters for simulations in this work.

Phase	Elastic modulus E (GPa)	Poisson's ratio ν	Surface energy γ (mJ/m^2)	Reference
Anhydrous cement grain	139.9	0.30	-	(Pichler and Hellmich, 2011)
Hydration product	29.2	0.24	50	(Bermard et al., 2003; Djouani et al., 2013)
Pore	0	0	-	-

4. Results and discussion

4.1. Damage evolution under uniaxial tensile loading

Fig. 5 illustrates the simulated stress-strain response for 28-day old cement paste under axial tensile loading. It can be seen that the initial elastic part is perfectly linear. Beyond the linear response, "graceful" quasi-brittle non-linearity prior to the last point is observed. The last point of the stress-strain curve corresponds to final failure. On basis of this curve, several macroscopic parameters of great concern, such as overall elastic modulus, tensile strength, strain at failure point and fracture energy of cement paste, can be gained. These parameters play crucial roles in the prediction of mechanical behaviours and fracture process of cement-based materials at the meso-level, i.e. mortar and concrete. The global elastic modulus corresponds to the slope of the stress-strain curve at the linear elastic stage. The tensile stress and strain at failure point are considered to be the tensile strength and peak strain, respectively. The fracture energy, that is an essential input to continuum-based fracture models, e.g. cohesive zone model, can be calculated as the area under the stress-strain curve. It denotes all energy loss resulting from distributed micro-cracking and eventual rupture divided by the cross-section area of cement paste specimen. Further insight into this process can be obtained from the development of the mechanical damage.

The evolution of the mechanical damage parameter D_E defined as a relative change in the material's elastic modulus is also shown in Fig. 5. In the beginning, D_E is very close to zero with few isolated local micro-cracks. As the deformation increases, the macroscopic damage starts to increase induced by the gradual local failure of bonds with larger pores in the cellular structure and growing population of micro-cracks. As introduced above, the bond fails when its energy reaches the assigned failure energy, mimicking the creation of a micro-crack along the interface between the two cells joined the bond. Upon failure the bond is removed from the site-bond assembly. This leads to a redistribution of forces in the structure and consecutive failures of bonds. The damage growth can be classified into two stages, the slow development stage and the rapid increase stage. The former can be explained by the continuous progress of isolate local failures till 1.5×10^{-4} applied strain. The bonds remaining in the cellular structure continue to carry the load. The latter is attributed to the coalescences of micro-cracks. A maximum damage of 8% can be observed at which the final failure of the cement paste specimen happens. This is a result of a simultaneous rupture of a set of bonds critical for the specimen integrity.

It is noted that the isolated local failures make a negligible contribution to the nonlinear stress-strain response. The clear non-linearity occurs along the micro-crack propagation and coalescence. The avalanche-failure results in the peak in the stress-strain curve, which corresponds to the separation of the whole structure into a collection of disjoint regions. The post-peak softening response is not observed under tensile loading. The main reason for this is

that the increments in the simulation are not small enough. To separate failing bonds close to the final failure of the specimen, short increments are required. This would result in an increase in computational cost.
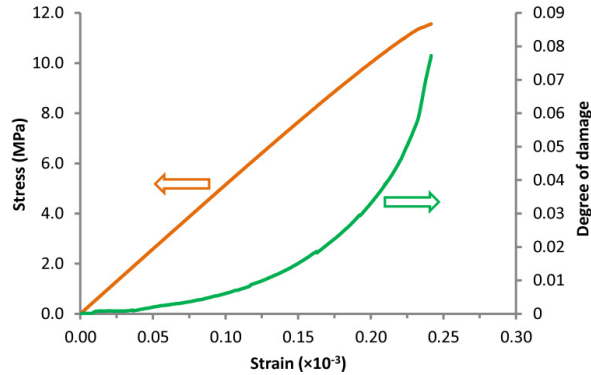

Fig. 5. Stress-strain response and damage evolution of cement paste under tensile loading.

4.2. Effect of porosity on tensile strength and damage evolution

To quantitatively investigate the effect of porosity on mechanical properties and damage evolution in cement paste, a series of samples with identical pore size distribution, volume fraction and size distribution of anhydrous cement grains but different porosities ranging from 8% to 35% are acquired. A set of 40 cement paste samples for respective porosity are simulated. Fig. 6 illustrates the average tensile strength against the porosity of cement paste. As expected the tensile strength decreases with the increase of porosity.

For the purpose of comparison, the experimental data of tensile strength as a function the porosity of cement paste taken from Chen et al. (2013) are also shown in Fig. 6. A correlation coefficient of 0.98 between the simulation results and experimental data is found, which indicates that the simulation results show a very good agreement with the experimental data, especially for the specimens with porosity higher than 20%.
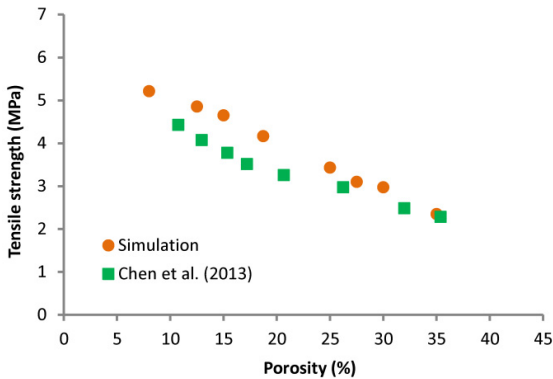

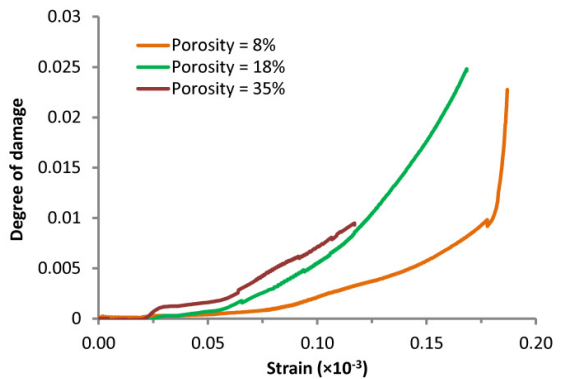Fig. 6. Tensile strength of cement paste against porosity.

Fig. 7. Damage evolution in cement pastes with different porosities.

Fig. 7 shows the rate of damage evolution with the increase of the applied strain for cement paste specimens with porosities of 8%, 18% and 35%. When the applied strain is small, no damage occurs in cement paste. As the applied strain increases, there is a gradual increase in the value of the damage parameter D_E. For the specimen with a higher porosity, the damage develops more quickly and the specimen fails earlier. This can be attributed to the fact that with the increase of the amount of pores the coalescence of bonds failed under loading (micro-cracks) seems to be

easier and more rapid. Prior to final failure, the specimens with porosities of 18% and 35% show a similar tendency in damage development. When the applied strain reaches about 0.18 ($\times 10^{-3}$), the rate of damage evolution in the 35% porosity specimen sharply increases. This corresponds to the sudden simultaneous rupture of bonds in the system.

5. Conclusion

This work presents a lattice-spring modelling of damage evolution in cement paste. The experimental microstructure of hardened cement paste acquired from high-resolution micro-CT is mapped to the site-bond assembly with anhydrous cement grains at each site and pores on the interfaces (i.e. bonds) between cells. Each bond is represented by a set of normal and shear springs, the stiffness coefficients of which are determined as a function of macroscopic elastic properties of components. From the findings of the present study, the following conclusions can be drawn:

- The macroscopic non-linear behaviour of hardened cement paste is captured as a result of the propagation and coalescence of local bonds of failure (i.e. micro-cracks) under loading. The rate of macroscopic damage evolution increases with the increase of loading, which reflects the significant dissipation of energy by distributed micro-cracking.
- Porosity plays a significant role in the mechanical properties and damage evolution. The simulated tensile strength-porosity relationship of cement paste shows a good agreement with experimental data. The specimen with higher porosity shows more rapid damage evolution and more brittle response under equal other conditions.

The developed lattice-spring model can be used to estimate the changes in mechanical properties and fracture energy of cement-based materials due to microstructural changes during aging.

Acknowledgements

References

Bernard, O., Ulm, F.J., Lemarchand, E., 2003. A multiscale micromechanics-hydration model for the early-age elastic properties of cement-based materials. Cement and Concrete Research 33, 1293-1309.

Chen, X., Wu, S., Zhou, J., 2013. Influence of porosity on compressive and tensile strength of cement mortar. Construction and Building Materials 40, 869-874.

Djouani, F., Chehimi, M.M., Benzarti, K., 2013. Interactions of fully formulated epoxy with model cement hydrates. Journal of Adhesion Science Technology 27, 5-6, 469-489.

Jivkov, A.P., Engelberg, D.L., Stein, R., Petkovski, M., 2013. Pore space and brittle damage evolution in concrete. Engineering Fracture Mechanics 110, 378-395.

Jivkov, A.P., Yates, J.R., 2012. Elastic behaviour of a regular lattice for meso-scale modelling of solids. International Journal of Solids and Structures 49(22), 3089-3099.

Jivkov, A.P., Morrison, C.N., Zhang, M.Z., 2014. Site-bond modelling of structure-failure relations in quasi-brittle media. 20th European Conference on Fracture, Trondheim, Norway, Paper #689.

Pichler, B., Hellmich, C., 2011. Upscaling quasi-brittle strength of cement paste and mortar: A multi-scale engineering mechanics model. Cement and Concrete Research 41, 469-476.

Schlangen, E., Qian, Z., 2009. 3D modeling of fracture in cement-based materials. Journal of Multiscale Modeling 1(2), 245–261.

Zhang, M., He, Y., Ye., G., Lange, D.A., van Breugel, K., 2012. Computational investigation on mass diffusivity in Portland cement paste based on X-ray computed microtomography (μCT) image. Construction and Building Materials 27(1), 472–481.

Zhang, M., Jivkov, A.P., 2014. Microstructure-informed modelling of damage evolution in cement paste using a site-bond model. Construction and Building Materials (under review).

Zhang, M., Morrison, C.N., Jivkov, A.P., 2014. A meso-scale site-bond model for elasticity: Theory and calibration. Materials Research Innovations (in press).